Volume 19 | Number 1 | 7 January 2019 | Pages 1–188

Lab on a Chip

Devices and applications at the micro- and nanoscale

rsc.li/loc

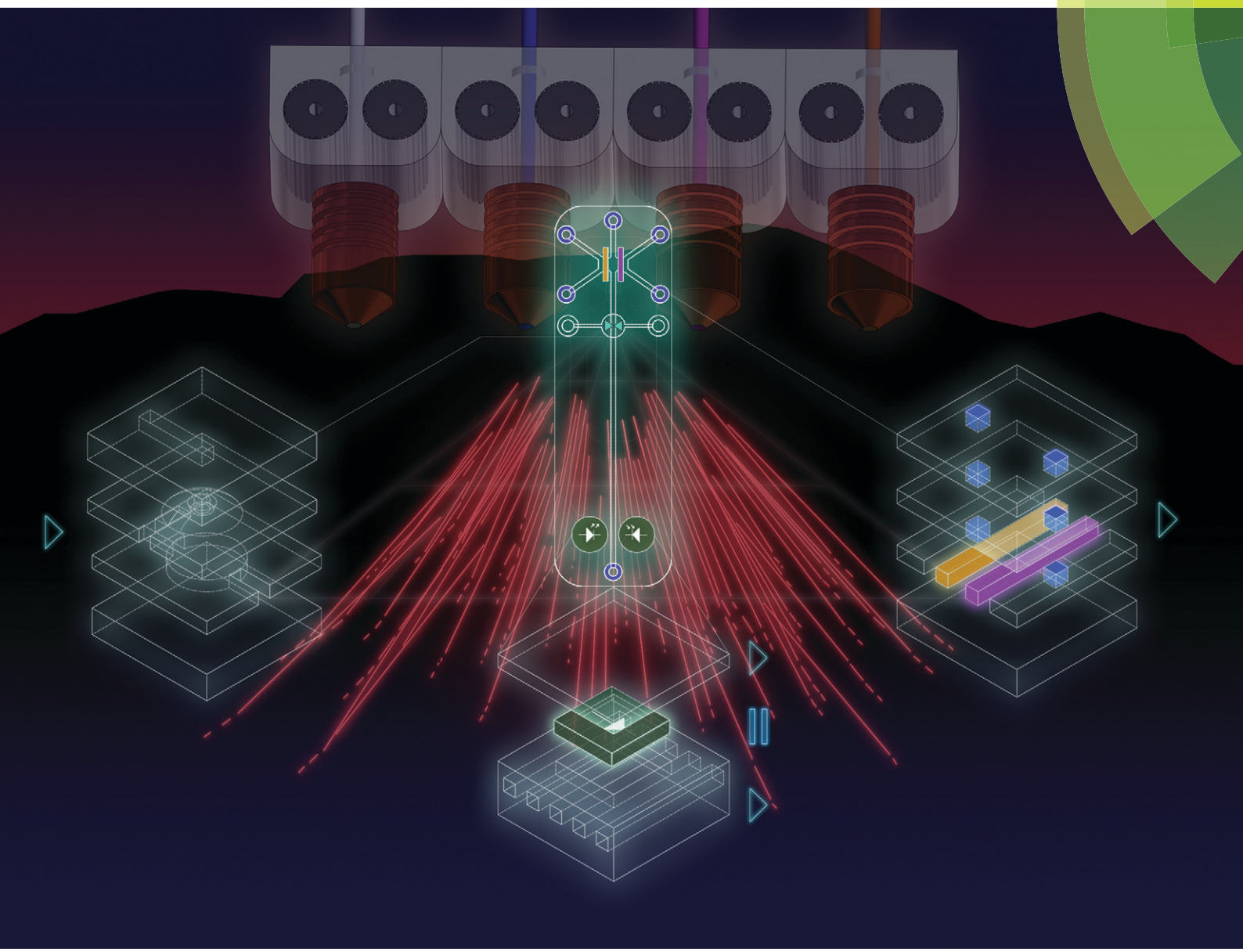

ISSN 1473-0197

ROYAL SOCIETY OF CHEMISTRY | Celebrating IYPT 2019

CRITICAL REVIEW

Michael C. Breadmore *et al.*

Increasing the functionalities of 3D printed microchemical devices by single material, multimaterial, and print-pause-print 3D printing

Lab on a Chip

CRITICAL REVIEW

View Article Online
View Journal | View Issue

Cite this: *Lab Chip*, 2019, **19**, 35

Increasing the functionalities of 3D printed microchemical devices by single material, multimaterial, and print-pause-print 3D printing

Feng Li,[a] Niall P. Macdonald,[cd] Rosanne M. Guijt [b] and Michael C. Breadmore *[a]

Received 10th August 2018,
Accepted 6th November 2018

DOI: 10.1039/c8lc00826d

rsc.li/loc

3D printing has emerged as a valuable approach for the fabrication of fluidic devices and may replace soft-lithography as the method of choice for rapid prototyping. The potential of this disruptive technology is much greater than this – it allows for functional integration in a single, highly automated manufacturing step in a cost and time effective manner. Integration of functionality with a 3D printer can be done through spatial configuration of a single material, inserting pre-made components mid-print in a print-pause-print approach, and/or through the precise spatial deposition of different materials with a multimaterial printer. This review provides an overview on the ways in which 3D printing has been exploited to create and use fluidic devices with different functionality, which provides a basis for critical reflection on the current deficiencies and future opportunities for integration by 3D printing.

1. Introduction

Integrated devices incorporate different functional components, performing multiple tasks in a single device. One of the best examples of an integrated device is an integrated circuit (IC), which was first reported by Kilby in the 1960s.[1] An IC is a small chip made with semiconductor material, normally silicon, with an integrated set of electronic circuits on it. Compared with the construction of discrete electronic components, ICs show huge advantages in cost and performance, attributing its dominating role in computers, mobile phones, and other electronic devices.

Inspired by the IC industry, microelectromechanical systems (MEMS) were developed as microsensors and microactuators, and for use in microsystems. Similar manufacturing techniques, such as photolithography, etching and deposition, were initially used to fabricate MEMS devices.[2] They normally have moving components, allow physical or analytical functions to be performed by the device in addition to their electrical functionality.[3] MEMS facilitated the development of the integrated microfluidic device (also called lab-on-chip or miniaturized total analysis systems) by Manz and co-workers in the early 1990s.[4] The integration of multiple distinct chemical and biological processes into a single device was anticipated to produce a similar revolution in chemistry and biology. Integrated microfluidic devices have been used in biochemical detection,[5–7] genetic analysis,[8–10] environmental analysis,[11–13] as well as for cell culture and organic synthesis.[14,15] Despite it being over 25 years since the introduction of these concepts, the number of integrated devices are few, partly due to the complexity and cost of their fabrication.[16]

Fabrication methods for microfluidic devices were initially inspired by the MEMS industry[17] but integrating components for microchemical systems has additional requirements to micromechanical systems. The integration of chemically functional materials may be incompatible with MEMS processing and the incorporation of liquid/solid chemical reagents poses a new challenge. It is therefore likely to add processing steps, often using complementary instrumentation and/or manual handling. From the manufacturability perspective, the number of processing steps should be minimized as these increase the likelihood of failure and rapidly decrease yield, resulting in an increase in cost.[18]

Three-dimensional (3D) printing, or additive manufacturing, is a layer-by-layer fabrication process developed in the early 1980s, that has over the past 5–10 years emerged as a promising approach for the fabrication of fluidic devices. Compared to conventional manufacturing methods, it is attractive for the fabrication of microchemical systems because of the more efficient fabrication of complex and bespoke designs, including those with integrated functionality, and the

[a] *Australian Centre for Research on Separation Science, School of Chemistry, University of Tasmania, Private Bag 75, Hobart, Tasmania 7001, Australia. E-mail: Michael.Breadmore@utas.edu.au*
[b] *Deakin University, Centre for Rural and Regional Futures, Private Bag 20000, 3220 Geelong, Australia*
[c] *Analytical-Chemistry Group, van't Hoff Institute for Molecular Sciences, University of Amsterdam, Science Park 904, 1098 XH Amsterdam, The Netherlands*
[d] *Vrije Universiteit Amsterdam, Division of BioAnalytical Chemistry, De Boelelaan 1108, 1081 HZ Amsterdam, The Netherlands*

ability to create truly 3D structures in a matter of minutes or hours.

The most widely used 3D printing techniques include stereolithography (SLA), fused deposition modeling (FDM), inkjet printing, laminated object manufacturing (LOM), selective laser sintering (SLS), and direct writing.[19,20] Each 3D printing technique has its own merits and drawbacks in terms of fabrication speed, resolution, accuracy, and cost; comprehensive comparisons have been made by some excellent reviews.[17,21–24]

This review will discuss the ways in which functionality can be integrated into a microchemical device. It is structured by way of integration: (1) single material 3D printing with functionality achieved through 3D spatial orientation of material, (2) temporary disruption of the print process to add additional components to integration, termed print-pause-print (PPP) approach by Pinger *et al.*[25] and (3) the precise spatial deposition of multiple-different materials *via* multimaterial 3D printing. Reviewed works are further categorized by the integrated functionalities: pumps, valves and mixers, electronics, modular microfluidics, membrane and porous structures, and chemical reactants. Table 1 summarizes integrated devices published to mid 2018, the most significant of which are discussed in more detail below.

2. Functionally integrated devices by single build-material printing

Currently, most 3D printed objects comprise of one single build material due to the technical difficulty in realising multimaterial printing, and – for most printing approaches – the limited range of materials available. Integrated functionality in single material 3D printed devices can be obtained by combining the 3D geometry and intrinsic material properties, such as elasticity or porosity. As discussed below, functional integration of single material devices has primarily focused on fluid control.

2.1. Valves, pumps, and mixers

Fluid manipulation underpins microchemical systems, making valves, mixers and pumps essential to their functioning. It is therefore not surprising that significant attention has focused on ways to control of fluid movement. Active control can be achieved through the integration of valves, with one of the first 3D printed valves presented by Rogers and co-workers. They fabricated a microfluidic device with integrated pneumatic valves capable of operating for 800 actuations. The valve consisted of a 100 μm membrane as part of a device 3D printed in a custom, flexible resin containing poly(ethylene glycol) diacrylate (PEGDA) using a SLA printer. The stiffness of a material scales with the square of its thickness, making the thin membrane more flexible than the thicker bulk of the device, allowing for localised deflection when an external pressure is applied. This deflection of the membrane was used for sealing the inlet and outlet openings, effectively closing the valve. When the pressure was released, the membrane returned to its original position, opening the valve.[26] To improve the longevity of the valves, Gong *et al.* modified the resin further by adding a thermal initiator to complete the polymerisation reaction post-print. The thermal post-cure was found to be more efficient and yield better printed structures than UV-initiated process. Improvements in both the resin chemistry and printer resolution allowed the valve volume to be reduced to only 10% of the initial report, while its durability was improved from 800 actuations to over 1 million. Further exploitation of the spatial arrangement of the material allowed multiple valves to be integrated to create a pump and micro mixer.[27] Au and co-workers also 3D printed microfluidic devices with integrated valves and pumps, with some of their devices shown in Fig. 1. The performance of the thin plastic valve to different pressure loadings was firstly simulated using COMSOL software to calculate maximum pressure before deformation, which was confirmed with experimental studies. 3D printed microfluidic devices with integrated valves and pumps were used for culturing and observation of CHO-K1 cells; facilitated by the optically transparency and biocompatibility of the 3D printing resin (Watershed XC 11122, DSM Somos).[28] Sochol *et al.* designed, simulated, and fabricated using multi-jet 3D printing, microfluidic circuit components including diodes, capacitors, and transistors as shown in Fig. 1. However, efficiency of the components was limited by micro features left by support-build material interaction causing the valves not to fully seal; diodicity 80.6 ± 1.8, transistor pressure gain 3.01 ± 0.78.[29]

Wang *et al.* used a FDM printer to integrate pneumatic micropumps and micromixer in a microfluidic device for chemiluminescent detection of insulin using the flexible thermoplastic elastomer (TPE). Comparable fluid control to that achievable using devices made by soft lithography in PDMS was demonstrated.[30]

Two-part valves and pumps actuated by rotating or torqueing were 3D printed using a SLA printer by Chan *et al.* The pumps and valves were printed as two parts – a screw and main chip – with flow controlled by rotating the screw by hand. Integration with microfluidic components facilitated a colorimetric assay for urinary proteins using a smartphone for imaging, with data processing performed on a laptop. The whole assay was done within 25 min, and chip cost of US$0.22 without any extra lab instruments. In comparison with a lateral flow assay, the 3D printed device is more complex and more expensive, but the quality of the data obtained using limited infrastructure highlights the potential of 3DP microfluidics to produce low-cost advanced point-of-care technology for resource-limited areas.[31]

Mixing of fluids is required for many processes, including chemical reactions,[32,33] and biochemical assays.[34,35] Mixing can be achieved by passive (diffusion, chaotic) or active (pumps, surface acoustic waves, internal moving components) methods.[36] The ability of creating complex geometries in a single manufacturing step makes 3D printing an

Table 1 3D printed integrated devices

Integration approach	Integrated functionality	Application/notes	3D printing technology	Print materials	Ref.
Single material 3D printing	Valve	Microfluidic valve for fluid control. 1.73 mm^3 fluid volume, 800 actuation in a single device	SLA	Customized resin	26
	Valve, pump, mixer	Fluid control. 0.165 mm^3 fluid volume, 1 million actuation in a single valve. 40 $\mu L\ min^{-1}$ maximum flow rate of the pump	SLA	Customized resin	27
	Valve, pump	Cell culture applications. 74.8 mm^3 fluid volume, 15 000 actuations in a single valve. 0.68 $mL\ min^{-1}$ maximum flow rate of the pump	SLA	WaterShed XC 11122 resin	28
	Fluidic circuitry	Fluid control	PolyJet	Visijet M3 Crystal	29
	Pump, mixer	Chemiluminescence immunoassay of insulin. 712.56 $\mu L\ min^{-1}$ maximum flow rate of the pump. 252 mm^3 fluid volume of the mixer	FDM	Flexible TPE	30
	Valve, pump	Colorimetric analysis of proteins in urine	SLA	BV-003 resin	31
	Mixer	Colorimetric detection of blood haemoglobin level. 4.32 mm^3 fluid volume, 20 $\mu L\ s^{-1}$ flow rate of the mixer	PolyJet	VisiJet® FTX Clear resin	37
	Mixer	Mixing of two dyes. 100 $\mu L\ min^{-1}$ flow rate of the mixer	SLA	BV-001 resin	38
	Mixer	Automated pK_a determination. 20 mm^3 fluid volume, 0.3 $\mu L\ s^{-1}$ flow rate of the mixer	SLA	BV-001 resin	40
	Mixer	Fluid control in microfluidics. 0.94 mm^3 fluid volume, 100 $\mu L\ min^{-1}$ flow rate of the mixer	FDM, SLA, PolyJet	ABS, BV-007 resin, Veroclear-RGD810	24
	Mixer	Colorimetric analysis of Fe^{3+} in water. 1.125 mm^3 fluid volume, 100 $\mu L\ min^{-1}$ flow rate of the mixer	FDM	ABS	41
	Porous structures	Extraction of trace elements in seawater	SLA	BV-001 resin	42
	Porous structures	TLC separation different dyes	Modified FDM	Silica gel	43
	Porous structures	Extraction of drugs from water	FDM	LAY-FOMM 60	44
	Porous structures	TLC separation different proteins	PolyJet	Veroclear-RGD810	45
	Modular microfluidics	Detection of AFP biomarker. 100–1000 μm in width and 50–500 μm in height of the microchannel. 30 × 30 × 5 mm (width × height × length) of the module units. 200 kPa maximum bearable pressure without leakage	PolyJet	VisiJet M3 Crystal	46
	Modular microfluidics	Microdroplet generator. 500 μm × 500 μm cross-sectional length of the microchannel. Maximum flow rate is 200 $mL\ h^{-1}$ without leakage	SLA	Somos WaterShed XC 11122 photoresin	47
	Modular microfluidics	"SmartBuild System" for biological and chemical applications. Microchannels are 635 μm in diameter. The maximum bearable pressure is 51.1 psi	SLA	UV cured resin	48
	Modular microfluidics	Reconfigurable stick-n-play microfluidic system. 1000 μm × 1000 μm cross-sectional length of the channel. Maximum bearable pressure is 26.3 psig	FDM	XT copolyester filament	49
Print-pause-print 3D printing	Mixer	3D printed reactor for online mass spectrometry monitoring of the chemical reaction. 250 mm^3 fluid volume, 125 $\mu L\ min^{-1}$ flow rate of the mixer	FDM	PP	51
	Electronics	Electronic tongue	FDM	PLA	52
	Electronics	pH and conductivity sensing for water monitoring	FDM	ABS	53
	Chemical reactants	3D printed reaction ware with printed catalyst chemical synthesis	FDM	PP, catalyst doped PP	54–56
	Chemical reactants	Synthesis of arylnaphthylalkynes with NMR spectroscopy	FDM	Polyamide	57
	Membrane	3D printed equilibrium-dialysis device for investigating the binding of small molecules and ions to proteins	PolyJet	VeroClear	25
	Membrane	3D printed device for continuous perfusion cell culturing	FDM	XT copolyester filament	58
Multimaterial 3D printing	Pump	3D printed pumping lid for controlling flow in droplet microfluidics and sample loading. 5 $mL\ min^{-1}$ maximum flow rate of the pump	PolyJet	VeroClear, TangoBlack	59
	Mixer	3D printed interlock meter-mix device for accurately sample metering. 1150 μL fluid volume of the mixer	PolyJet	VeroClear, TangoBlack	60
	Valve	Microfluidic valve	PolyJet	VeroWhitePlus, TangoBlack	61
	Electronics	Measuring the size of microdroplets *via* capacitively coupled contactless conductivity detection (C4D) detection	FDM	CNT-doped PLA	62

Table 1 *(continued)*

Integration approach	Integrated functionality	Application/notes	3D printing technology	Print materials	Ref.
	Electronics	Voltammetric sensing of heavy metals in water	FDM	Polystyrene, conductive filament	63
	Electronics	3D printed electronic sensors for sensing mechanical flexing	FDM	Carbon black contained filament, PLA	64
	Magnet sensor	3D printed impeller flow sensor	FDM	Magnet filament, ABS	65
	Electronics	ITP of bacterial	FDM	ABS, cabon doped ABS	66
	Electronics	3D printed lithium battery	Modified FDM	Customized materials	67
	Electronics	Electrochemical energy storage	Modified FDM	Copper and graphene	68
	Chemical reactants	3D printed reaction ware with printed catalyst chemical synthesis	Modified FDM	Acetoxysilicone	69
	Chemical reactants	Direct soil nitrate detection	FDM	ABS, LAY-FELT	70
	Chemical reactants	Glucose assay	FDM	Customized ABS-based filament	71
	Interconnect	3D printed diffusion based device for *in vitro* pharmacokinetic study. 2000 μm × 2000 μm cross-sectional length of the channel	PolyJet	VeroClear, TangoBlack	72
	Interconnect	3D-printed microfluidic chip with interconnects. 250 μm × 250 μm cross-sectional length of the channel. The maximum bearable pressure is 416 kPa	PolyJet	VeroBlack, TangoBlack	73
	Interconnect	Monitoring real-time subcutaneous glucose and lactate levels. The minimum microchannel is 520 μm × 520 μm in width and height. The internal fluid volume is 1.91 μL	PolyJet	VeroWhitePlus, TangoBlack	74
	Interconnect	Amperometric detection of H_2O_2. 800 μm × 800 μm cross-sectional length of the channel. The maximum flow rate is 2000 μL min^{-1}	FDM	ABS, PET	75
	Interconnect	Microfluidic droplet generation. The minimum microchannel is 239 μm in diameter. The maximum bearable pressure is 4 bar	PolyJet	VeroClear TangoPlus FLX930	76

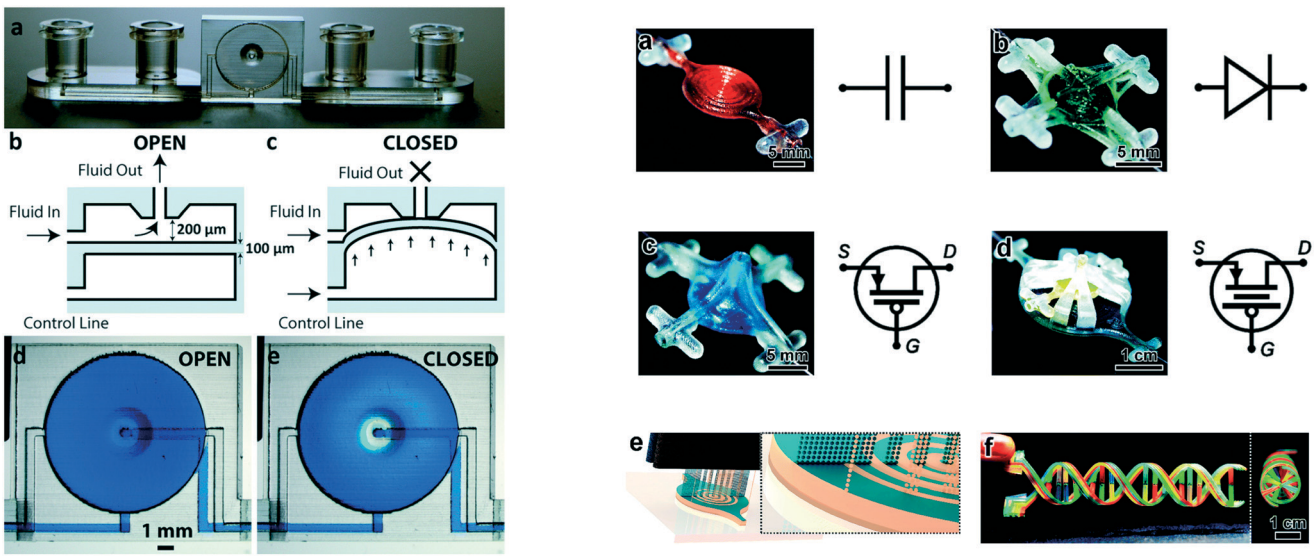

Fig. 1 (Left) Basic valve design. (a) Photograph of the single-valve device. (b and c) Schematics of a valve unit in its open (b) and closed (c) states. (d and e) Micrographs of a valve unit in its open (d) and closed (e) states. (Right) 3D printed fluidic circuit components. a) Fluidic capacitors, b) fluidic diodes, c) fluidic transistors, d) enhanced-gain fluidic transistors, e) conceptual illustration of the MJM process for simultaneous inkjet deposition of photoplastic (blue) and sacrificial support (beige) materials, f) a 3D printed DNA-inspired architecture comprised of eight fluidic channels (750 μm in diameter) filled with discrete solutions of dye-coloured fluid reproduced from ref. 28 and 29 with permission.

efficient and simpler way to fabricate mixers when compared to traditional fabrication methods. A ring-shaped channel architecture combining a 'Slit and Recombination (SAR)' structure with serpentine channels was presented for fast (~1 s) and complete fluid mixing. Fluid flow in the chip, fabricated using a PolyJet printer, was driven by capillary action, and there was good agreement between experimental results and CFD simulations. By integrating this chip with a smartphone, the mixing device was used for point-of-care diagnosis of anaemia by colorimetric quantification of blood hemoglobin levels.[37] Shallan *et al.*[38] fabricated a micromixer based on Baker's transformation using a desktop DLP–SLA printer.[39] This mixer was subsequently used to mix four reagents to create a rapid and automated method for the determination acidity constants (pK_a) of pharmaceuticals.[40]

As an alternative to designing complex channel geometries, fluidic mixing can also be the result of surface topography inherent to the printing process. Macdonald *et al.* compared the fluidic properties of SLA, FDM, and PolyJet printed microfluidic devices using a simple "Y" shape geometry. The highest degree of mixing was observed in FDM printed devices, followed by PolyJet and SLA.[24] Li *et al.* explored the impact of FDM printing orientation relative to the flow path on mixing behaviour as shown in Fig. 2. Different printing orientations (0°, 30°, 60°, 90°) of the filament to the direction of the fluid flow were compared using the same "Y" channel design. Chips printed with the filament extruded at a 60° angle to the flow path were found to be optimal for fluid mixing, and were used to detect iron in water by colorimetric assay.[41]

2.2. Porous structures and membranes

Porosity increases the surface area and controls material transport properties. Chromatography relies on the interaction of analytes with a stationary heterogenous phase, favouring porous materials owing to their high surface area. Combining surface chemistry and design, a 3D printed solid-phase extractor with ordered cuboids to improve liquid–surface contact was developed by Su and co-workers. The device contained 526 cuboids (0.4 mm × 0.4 mm × 0.2 mm (length × width × height)) in the channel and was created using a SLA printer. The extraction of the metal ions from solution was achieved by interactions between the polymer material and metal ions. The extraction system was coupled to ICP-MS for metal ion quantitation.[42] While this demonstrates promise, the printer resolution is insufficient to provide similar performance to that obtained with conventional solid-phase extraction materials and columns.

Fichou and co-workers printed a planar chromatography system using a silica gel slurry. A FDM printer was modified to directly print the silica gel with a slurry doser designed to replace the plastic extruder of a Prusa i3 printer. The separation performance of this chromatography system of different dyes was comparable to a commercial TLC plate. Benefiting

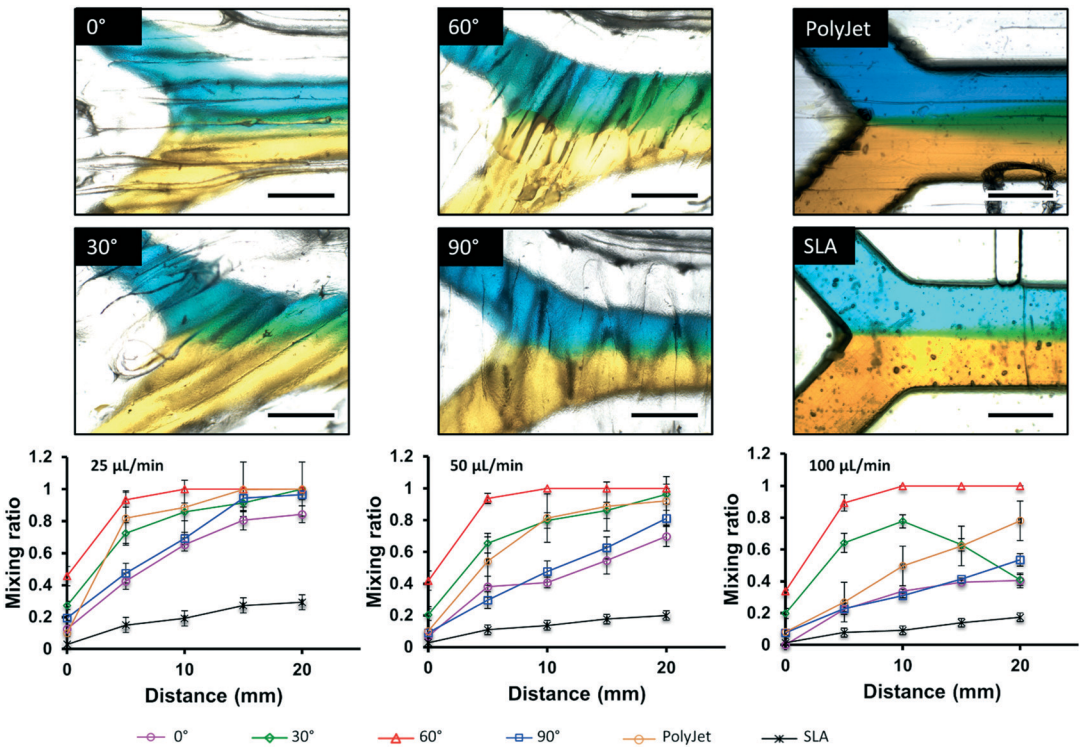

Fig. 2 Microscopic images of laminar flow within 500 μm × 500 μm channels into 750 μm × 500 μm channels, visualized with yellow and blue food dye at 25 μL min^{-1} for FDM 0°, 30°, 60°, and 90°, Polyjet, and SLA, respectively. Plots of distance *vs.* mixing ratio, demonstrating diffusion through the laminar flow channel at 25, 50, and 100 μL min^{-1} are also shown below the microscopic images. N = 3, scale bar = 500 μm. Reproduced from ref. 41 with permission.

from the freedom of the 3D design, this method offers new opportunities in terms of geometry, shape and functional integration; potentially allowing from an extending from 2D to 3D chromatography.[43] Belka and co-workers created an extraction unit to concentrate pharmaceuticals by FDM printing in LAY-FORMM 60, a material which becomes porous after removal of a water-soluble support by washing with water. The printed tube-shaped sorbent was placed within an Eppendorf tube for centrifuge extraction of glimepiride from water, reporting the extraction efficiency of 82.24% after 60 min.[44]

Macdonald *et al.* printed a microstructured surface for planar chromatography using a PolyJet 3D printer by exploiting phenomena that occurs during the print process. When printing fine structures, mixing between the support and build materials prior to polymerization leads to the creation of 3D microstructures, as shown in Fig. 3. When the support material is removed, a porous layer of tens of microns thick is created, which can be used for chromatography. Optimum chromatographic performance was achieved using devices printed parallel to the print head movement, as characterized by shorter separation times and reduced interferences between adjacent channels. The negatively charged surface was used for the separation of water-soluble dyes, phenol red and bromothymol blue, and proteins, myoglobin (pI 6.8, 7.2) and lysozyme (pI 11.35).[45]

2.3. Fluidic interconnects and modular systems

One of the most common ways of creating more complex fluidic devices has been to create individual modules that can be fluidically connected to configure a range of microchemical systems.[46–49] Inspired by electronic circuit prototyping using breadboards and Lego®, Yuen presented a "plug-n-plug" modular microfluidic system. The "Smart Build System" comprised multiple microfluidic components fabricated *via* a SLA printer. Various microfluidic elements including a motherboard with fluidic interconnects, fittings, and fluidic inserts were 3D printed individually before their assembly into a system.[48] Yuen presented a "stick-n-play" modular microfluidic system incorporating magnets and sealing gaskets to reversibly 'stick' modules together.[49] Lee and co-workers[46] and Bhargava and co-workers[47] constructed functionally integrated microfluidic devices including a gradient generator, microdroplet generator and optical droplet sensing system by connecting SLA printed fluidic units such as mixers, splitters, junctions, *etc.*

3. Functionally integrated devices by print-pause-print (PPP) 3D printing

The simplest way to overcome the limitations imposed by printing in a single material is the PPP approach to printing. Most 3D printers operate in a layer-by-layer manner, providing an opportunity to be paused mid-print, *i.e.* between layers, to insert external elements or to hyphenate with a complementary fabrication processes to create hybrid devices. Hybrid 3D printing can also include traditional, subtractive manufacturing methods such as machining, cutting, dispensing, and robotic placement.[50] By taking advantage of the geometric benefits of 3D printing, and integrating other components into the fabrication process, additional functionality can be included in the final device. PPP is highly attractive for the incorporation of sophisticated electronic or optical functionality, but may not be suitable for all 3D printing approaches. PPP is most frequently used in combination with FDM 3D printing.

3.1. Valves, pumps, and mixers

In this regard, reports of integrated fluidic functionality by PPP is currently limited. Scotti *et al.* FDM printed a polypropylene reactor using the PPP approach with a magnetic stir bar and an integrated stainless steel capillary for nano-electrospray ionisation for direct injection into a mass spectrometer. The device was used for monitoring a Diels–Alder reaction and the subsequent retro Diels–Alder reaction.[51]

3.2. Sensors and electronics

Given a significant focus of microchemical systems is on analysis, it is no surprise that there has been a strong focus

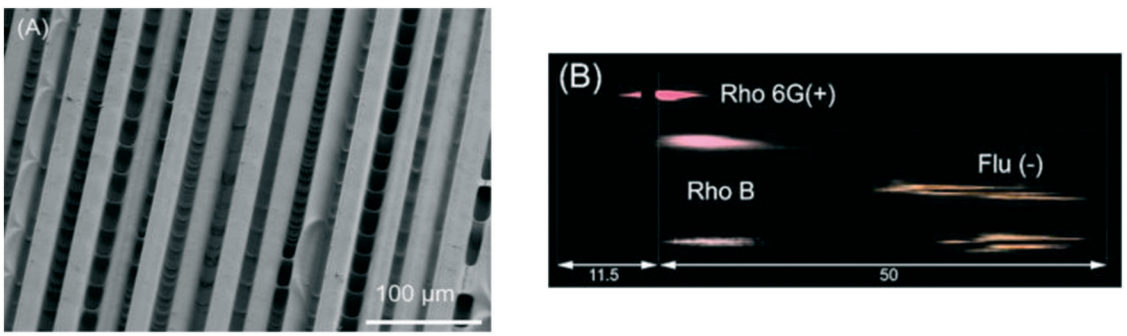

Fig. 3 3D printed TLC chip showing separation of rhodamine 6G (Rho 6G), rhodamine B (Rho B), and fluorescein (Flu). (A) Scanning electron microscopic (SEM) images of 3D printed TLC chips of 200 μm thickness. Substrate of separation chip showing parallel microchannels (11.9 μm ± 2.9 μm, n = 12) corresponding to the printer head orientation, taken at ×300 magnification. (B) Processed photograph with the background removed showing the separated dyes only. Reproduced from ref. 45 with permission.

on the integration of electronic functionality for sensing/detection. A PPP method was developed for the fabrication of a 3D printed electronic tongue using an FDM printer. A transparency containing gold inter-digitated electrodes (IDEs) was embedded within a 3D printed PLA microchip for taste sensing. The PLA microchannel was 600 μm in width and height, with a square chamber having the same height and 5 mm in width, designed to fit the IDEs. The electrical response from the electrodes were acquired using an impedance analyzer, and analyzed using principal component analysis. The 'tongue' was able to distinguish between NaCl, HCl, caffeine and sucrose solutions showing a 99.98% correlation of tastants.[52] An integrated water quality monitoring system containing miniaturized pH and conductivity sensors was fabricated by PPP. The conductivity sensor comprised of two interdigitated electrodes, and the pH sensor was a combination of interdigitated electrodes with a hydrogel. The pH-induced swelling of the hydrogel was measured by the interdigitated electrodes as a change in the electrical properties (conductivity and capacitance).[53]

3.3. Chemical reactants

One of the attractions in FDM printing for PPP is the fact voids remain empty, and in addition to inserting components, this can be used to introduce chemical reagents. This is in contrast with inkjet printing, where a solid support material is used, or SLA/DLP where unpolymerized resin stays in the voids. PPP for incorporating chemical reagents was first demonstrated by Cronin *et al.* who made 3D printed reactionware with integrated solid and liquid reagents for chemical reactions (Fig. 4). Kitson *et al.* was the first to demonstrate the utilization of PPP for solid reagent integration. Two different solids, sodium molybdate and hydrazine dihydrochloride, were incorporated in two connected containers during the PPP. A solution was then be introduced into the reactor by a single inlet and flowed through the device dissolving the first solid, and then the other reactant to induce a chemical reaction.[54] Liquid reagent integration through PPP was also achieved by Kitson *et al.* By using this method, multi-step reactions were conducted with minimal chemical handling by the operator, allowing complex manipulations to be precisely controlled, optimized, and shared and repeated by other researchers. This approach has subsequently allowed the fabrication of customized chemical reactors which can be tuned by individual researchers.[55,56] Using a 2-printer approach, Kitson *et al.* created 3D printed catalytic microreactors. After printing the polypropylene (PP) reactor using an FDM printer, a Fab@Home extrusion printer was used to deposit PP blended with catalyst materials (Lewis catalyst and Pd/C, respectively). After addition of liquid reagents, the polypropylene FDM printing process was resumed, as illustrated in Fig. 4. The devices were used for a multistep reaction, with fluidic transport facilitated by rotation of the device.[56]

Lederle and co-workers 3D printed a NMR tube/spinner combination with integrated reactants inside the inert-gas atmosphere of a glovebox for palladium-catalyzed decarboxylative Sonogashira coupling of aryl halides with arylpropionic acids. Within the totally gas tight and pressure resistant tubes, a set of arylnaphthylalkynes was synthesized and the progress of the reaction was monitored *via* NMR spectroscopy.[57]

3.4. Porous structures and membranes

Porous membranes are selective barriers and allow for the extraction of analytical targets from complex mixtures. They are popular in separation science, and a wide range of commercially available membranes have been developed for a myriad of applications. The PPP method has been used for the incorporation of these specialist membranes in microchemical devices. A dialysis membrane was embedded for studying the binding of small molecules and ions to proteins. The window shaped membrane holders, shown in Fig. 5, were printed by inkjet printing using a combination of rigid and rubber-like materials, and when exactly half of the membrane holder was printed, the print process was paused manually and the pre-cut commercial dialysis membranes were inserted, and then the printing was resumed to finish the printing process. The

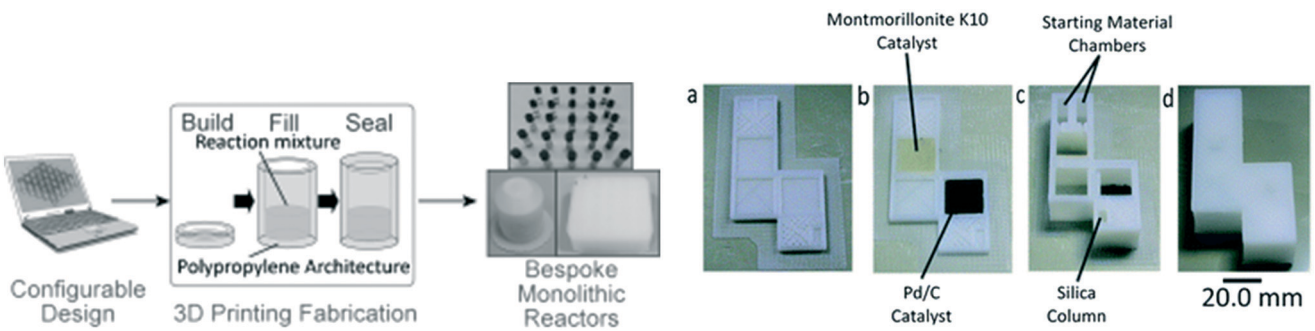

Fig. 4 (Left) The laboratory manufacturing process of 3D printed sealed reactors for hydrothermal synthesis. (Right) (a) Reactor base with purification column before printing of catalyst regions. (b) Reactor base with purification column after printing of catalyst regions. (c) Fabricated reactor with purification column after addition of starting materials, reagents and packing of silica. (d) Final sealed reactor. Reproduced from ref. 55 and 56 with permission.

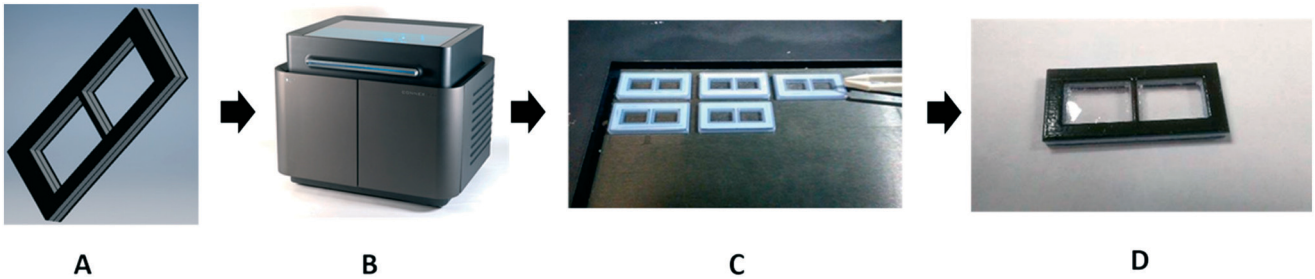

Fig. 5 In panel (A), a model is drawn using Autodesk Inventor Professional 2017 CAD software. The model is saved as an .stl file and sent to the 3D printer (panel (B)). The membrane holder is printed with multiple materials. The interior is a rigid Verowhite material, and the exterior is a compressible TangoBlack material, to prevent leaking. In panel (C), the operator places the membranes into the device halfway through the print process. Panel D shows the final product: a membrane holder with a membrane seamlessly sealed into the device. Reproduced from ref. 25 with permission.

advantage of this method is that membranes with different molecular weight cut-off can be embedded for different applications. Users of this approach should be aware, though, that the support material used in inkjet printing may be difficult to remove and change the membrane properties due to contamination of the membrane when resuming printing.[25]

Yuen used PPP for the fabrication of various fluidic devices with integrated porous membranes or light-diffusing fibers. A 3D printed fluidic device with an embedded porous membrane was used for continuous perfusion cell culture, and the integrated light-diffusing fiber offered opportunities in illumination or optical applications.[58]

4. Functionally integrated devices by multimaterial 3D printing

The pinnacle of integration by 3D printing is to be able to spatially deposit different materials during the print for fully automated fabrication of complex 3D functional devices. While conceptually simple, it requires printers that can precisely deposit small amounts of different materials in an accurate and reproducible manner and it also relies on materials with different functionality being available for that type of printer.

4.1. Valves, pumps, and mixers

Given the importance of fluidic control, it is not surprising the availability of commercially available flexible materials for inkjet printers has led to the incorporation of flexible elements for fluidic control in functionally integrated 3D printed devices. Begolo *et al.* utilized a multimaterial inkjet 3D printer to fabricate a pumping lid for equipment-free pumping using a rigid and a flexible material. The first version of the lid produced predictable positive/negative pressure by controlling the compression/expansion of a gas. A theoretical model was developed to describe the pressures and flow rates generated with this approach, which was validated experimentally. The second version of the lid relied on vapor–liquid equilibrium to generate pressure, and was validated by controlling flow into droplet microfluidics, laminar flow chips, and for loading sample in commercially available microfluidic chips.[59] However, the pumping lid they developed was only used to compress air, and was not applied to pump aqueous liquids directly. Jue and co-workers subsequently used a similar approach to fabricate an interlocked meter-mix device as shown in Fig. 6. This meter-mix device can generate sealed fluid cavities for accurately metering of urine before completely mixing it with lysis buffer. This type of device has potential in point-of-care analysis in resource-limited areas.[60]

Keating *et al.* used a polyjet printer with both flexible and rigid materials to create valves. Compared with the previously reported single material valve, this multimaterial valve showed stronger resistance to deformation. The valve showed proportional control over a flow rate ranging from 0 and 50 $\mu L\ s^{-1}$ without deformation. The application of this valve in DNA assembly and analysis, continuous sampling and sensing, and soft robotics is expected.[61]

4.2. Sensors and electronics

The ability to print conducting material presents the possibility to integrate electrical functionality into devices. Duarte and co-workers 3D printed a microfluidic device with embedded electrodes for generating, and measuring the size of microdroplets based on capacitively coupled contactless conductivity detection (C4D). The electrode was firstly printed with carbon nanotube-doped PLA in the bottom layer of the device, and then the filament was replaced by ABS to proceed with fabrication of microchannels through the same printing nozzle.[62]

Rymansaib and co-workers 3D printed an electrochemical device using polystyrene and an in-house carbon nanofiber (CNF)-graphite doped polystyrene (PS) with a dual-head FDM printer as shown in Fig. 7. The authors optimized the conductive composite material formulation, testing different base materials including ABS, polycaprolactone (PCL), and PS, with CNF and graphite. PS was chosen as the base material as ABS or PCL based composites gave poor response, possibly due to interfacial wetting effects. Printing the device in PS also ensured material compatibility during the print

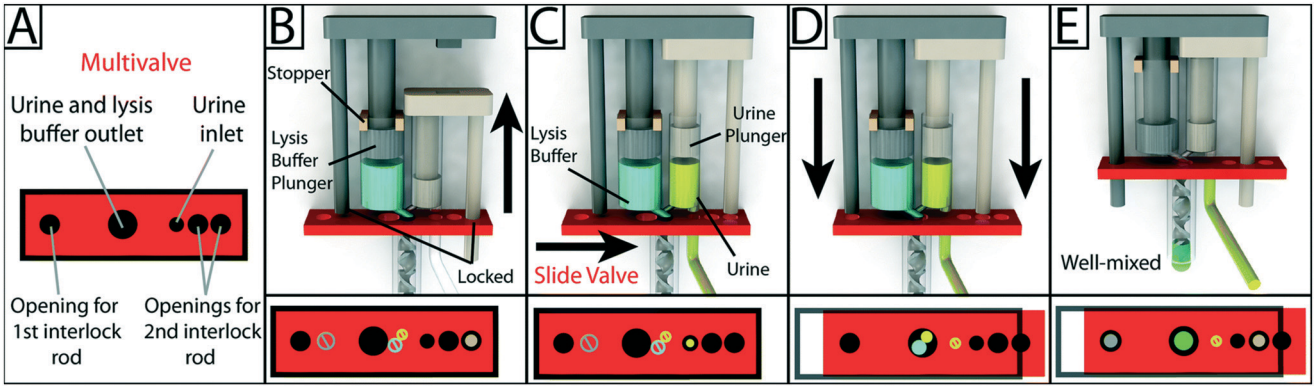

Fig. 6 Schematic overview of the design and operation of the 3D-printed interlock meter-mix device for metering and mixing a urine sample with lysis buffer. (A) The multivalve has five holes that are labeled accordingly. (B) Lysis buffer (blue) is preloaded into the lysis buffer chamber, where the topmost position of the lysis buffer plunger (left, grey) is pre-determined by stoppers (tan). The urine plunger interlock rod (right, beige) is positioned within the multivalve, preventing the valve from sliding and simultaneously blocking the lysis buffer plunger interlock rod. The user pulls up on the urine plunger (C) until it contacts and is stopped by the lysis buffer plunger, aspirating urine and simultaneously removing the urine plunger interlock rod from the multivalve. The user slides the multivalve (D), closing off the urine suction tube, opening the lysis buffer and urine outlets to the mixer, and providing openings for both interlock rods. In the final step, the user pushes down on the lysis buffer plunger (E), ejecting urine and lysis buffer through a static mixer, wherein the solutions are well mixed before finally being ejected from the tip of the mixer. Red blocks at the bottom of each panel show a top-down view of the multivalve. Black circles and rings indicate holes in the multivalve. Slashed circles indicate the presence of a feature that is blocked by the multivalve. Colored circles indicate the presence of an interlock rod or an open channel for the flow of a solution. Reproduced from ref. 60 with permission.

process, overcoming the delamination and adhesion challenges of multimaterial FDM printing. The device was used for cyclic voltammetry of aqueous 1,1′-ferrocenedimethanol and differential pulse voltammetry detection of aqueous Pb^{2+} *via* anodic stripping.[63] Conductive materials were also 3D printed and integrated with other supported parts using a three-head FDM printer to create mechanical flexing sensors. The electrode was printed with a customized conductive filament (termed 'carbomorph') using one of the nozzles, and the supporting parts were printed using the other two nozzles.[64]

An impeller flow sensor was fabricated with multimaterial FDM printing, the main body of the sensor was printed with ABS to maintain the structural integrity of the impeller, and a magnetic filament was printed on the top surface of the ABS body to allow for sensing of the flow rate. The 3D printed flow sensor showed comparable performance with commercial sensor in terms of the linearity of its response and repeatability.[65]

In a different use of conductive materials, Phung and co-workers 3D printed a fluidic device with integrated electrodes to provide a high voltage for isotachophoresis (ITP) of bacterial cells. The device was printed using a dual-head FDM printer, with ABS for fluidic device fabrication and carbon-based ABS for electrodes fabrication. The 3D printed electrode had a 0.3 MΩ higher resistance when compared to Pt electrode, which reduced the highest voltages available for electrophoresis, but the authors still successfully used this device for carry on a stable ITP experiment for bacterial cells.[66]

While much of the focus of 3D printing so far has been on analytical devices and sensing, Park and co-authors 3D printed a three-layer lithium battery for energy storage. The anode, electrolyte, and cathode were sequentially printed using different conductive cellulose composites using the combination of a commercial FDM 3D printer and a paste extrusion system to enable simultaneous printing of different parts. The battery had an open circuit voltage of 0.32 V, and full cell potential was around 1.8 V after charging for 4.5 h, which agreed with the reported cell voltages of 1.5–1.8 V of conventional batteries made with the same electrode materials. This study provides a potential for full-printed battery with conductive materials by 3D printing. 3D printing may rapidly design, prototype, and fabricate batteries with desired structures and shapes that can fit different electronic devices such as cell phones or laptops, 3D printing also enables the creation of devices with integrated batteries for multifunctional

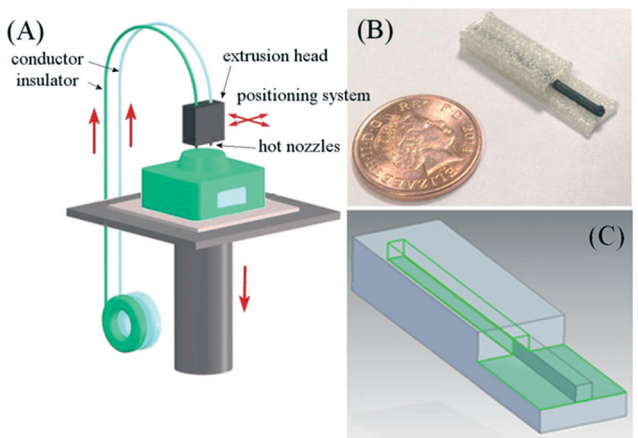

Fig. 7 (A) Schematic diagram of a 3D printing set up with two feeds (polystyrene insulator and polystyrene composite conductor) being printed through a hot nozzle system with positional controller. (B) Photograph of a printed polystyrene–nanocarbon composite electrode. (C) Multi-part electrode being designed in CAD software. Reproduced from ref. 63 with permission.

purposes by multimaterial 3D printing[67] Rocha *et al.* printed a graphene based device, also for energy storage. This device was fabricated using an aqueous-based thermoresponsive formulation including a chemically modified graphene (CMG) as the active material and copper as current collector. After printing, the printed device was frozen in liquid nitrogen and freeze-dried for 48 h, followed by thermal reduction at 900 °C for 1 h. Using this device, the specific energy and power densities reached values of 26 W h kg^{-1} and 13 kW kg^{-1}, and the device has promising long-term stability.[68]

4.3. Chemical reactants

By depositing chemicals during printing, reactionware and assay devices can be fabricated. The Cronin group introduced 2 material extrusion printing for the fabrication of integrated devices. Using a Fab at Home extrusion printer with two syringes, acetoxysilicone devices were printed containing acetoxysilicone-based blended materials for electrochemical and catalytic activity, respectively.[69]

A multimaterial FDM printer was used to fabricate a microfluidic device with a printed integrated membrane by Li *et al.* Liquid reagent was also embedded into the device, as shown in Fig. 8, making it suitable for the direct analysis of nitrate in soil. The integrated membrane was 3D printed with a commercially available porous composite (Lay-Felt®), eliminating additional processing steps and maintaining an automated fabrication pathway.[70]

Su and Chen presented microtiter plates with integrated reagents for a glucose assay printed using a dual head FDM printer using two customized filaments, for read-out on a plate reader. Filaments were customized using two different approaches, the chromophore was impregnated in PVA for controlled release upon exposure to water, and the catalyst-containing filament was blended and extruded in house. Here, peroxidase-mimicking Fe_3O_4 particles were blended with ABS for extrusion of a catalytic filament. The ratio and orientation of the two reagent-containing filaments was optimized and printed in a 96 well plate geometry, flued onto a polystyrene base. The devices allowed for enzymatic glucose assays between 5 and 500 μM and allowed for the detection of glucose in urine and plasma samples.[71]

4.4. Fluidic interconnects and modular systems

The ability to print both rigid and flexible materials allows the creation of fluidic connections with an integrated gasket to interface with other fluidic components. Lockwood and co-workers 3D printed an optically transparent device body with a flexible 'O-ring' to provide a liquid-tight seal to a Transwell insert containing a porous membrane. The device was printed with a rigid (VeroClear®), and flexible (Tango Black Plus) materials and contained six flow channels with wells above the channels into which the membrane insert was placed.[72] Using the same type of 3D printer and materials, a microfluidic chip interconnect composing of clamp and gasket was fabricated. This interconnect showed the ability to withstand pressure above 400 kPa.[73]

A slightly different interconnect was printed by Gowers *et al.*, using a second, compressible material to ensure

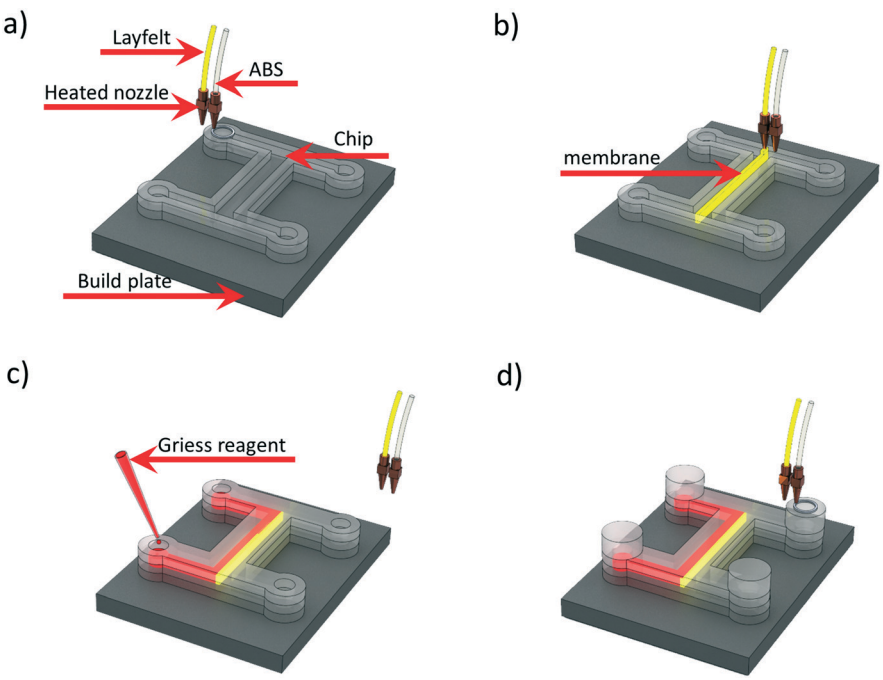

Fig. 8 Schematic of embedding Griess reagent during 3D printing process. (a) Chip printing with ABS. (b) Membrane printing with Lay-Felt. (c) Embedding Griess reagent while pausing the printing process. (d) Continuing printing to seal the reservoir. Reproduced from ref. 70 with permission.

sealing between the microfluidic and sensor-holding parts of a wearable device. The microfluidic structure as well as the holders or threaded ports for accommodating electrodes and biosensors were 3D printed, with the sensors inserted through the ports post-print. The integrated device was used for real-time monitoring of subcutaneous glucose and lactate levels in athletes during sports activities.[74]

A 3D printed fluidic device with threaded ports allowed integration of PEEK tubing and electrodes. The fluidic device was printed using polyethylene terephthalate (PET), and threaded fittings were printed with ABS. This device was used to prepare Prussian blue nanoparticles, which were then attached to gold electrodes for hydrogen peroxide sensing, and a limit of detection of 100 nM was achieved.[75]

Ji *et al.* also demonstrated the use of Polyjet to fabricate multimaterial modules for droplet generation as shown in Fig. 9; VeroClear material for structures and TangoPlus FLX930 for a 3D coaxial flexible channel. The flexible channel could be deformed by air pressure excitation, allowing for translation of actuation for multiple emulsion droplet generation.[76]

5. Challenges and future opportunities

Microchemical systems require complex, integrated functionality, a need that is not met by current, established fabrication approaches. 3D printing is a potential solution, but it must be recognized that this manufacturing path is still in its infancy – challenges remain in technology, material choice and throughput for all 3D printing approaches.

Across all of the approaches used to date, the realized print resolution barely matches that of conventional microfabrication approaches, which translates to larger microchannels (typically >200 μm in all dimensions). The only 3D printers competing on resolution are based on two photon polymerization (2PP) and while they can print devices down to nm features, the process is slow, build areas are in mm^2, and the high setup cost limits uptake.[77] This perfectly highlights the tradeoff between resolution, build space and print speed, for which there is currently no solution. Improvements are however being made. Gong *et al.* has provided a comprehensive study on improving 3D printable channel dimensions by optimizing the resin formulation with UV absorbers and adaptation of dose distribution. In doing so, they achieved 18 × 20 μm ($W \times D$) microfluidic channels using a custom made DLP–SLA system, however build space is reduced to 19.35 × 12.10 × 80 mm, *XYZ*,[78] smaller than what is normal for SLA printers.

FDM printing suffers critically as the machine resolution in the *XY* axis is significantly greater (≅300 μm) than what can be achieved with SLA (≅10 μm) and inkjet (≅50 μm). There are also fundamental questions about whether FDM printing can be made to extrude ever-smaller filament to achieve the micron-sized features that are desired for so many applications. Likewise, inkjet printing currently has limitations with resolution, exacerbated by the difficulty of the removal of the support materials from small features.

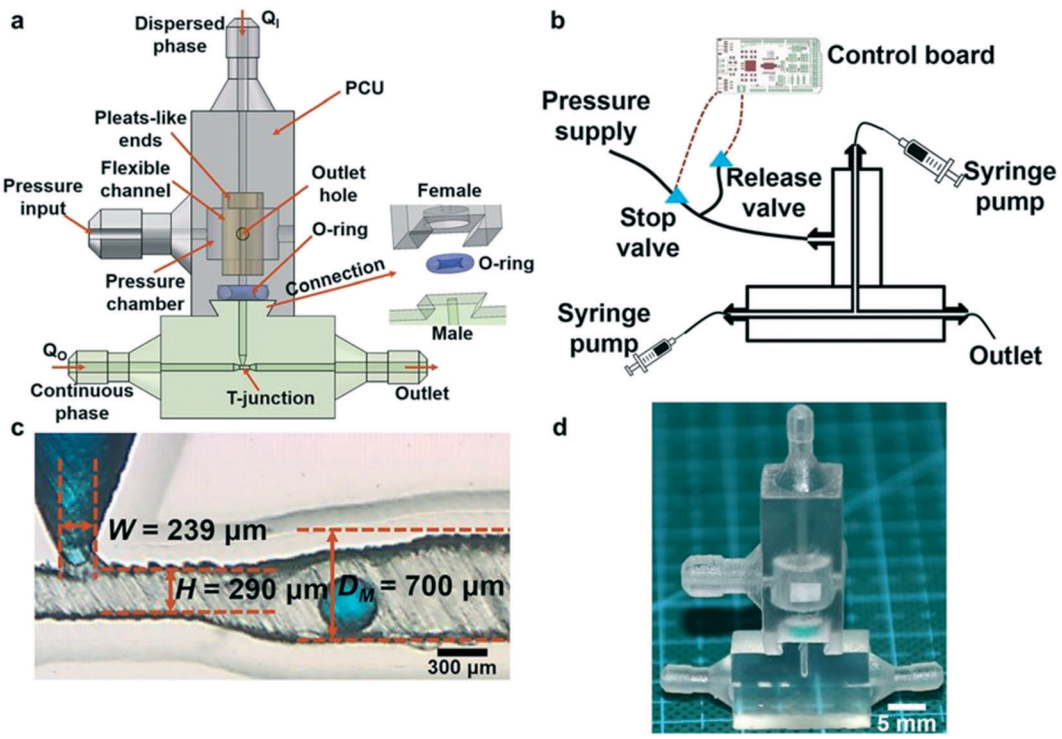

Fig. 9 (a) Schematic of the pneumatic device for droplet generation. (b) Schematic of the experimental setup. (c) Photograph showing T-junction channel. (d) A printed pneumatic device for emulsion generation. Reproduced from ref. 76 with permission.

The implementation of 3D printing in the fabrication of microchemical systems is also hindered by the limited choice in materials. The material choice in inkjet-based printers is restricted by the proprietary nature of the print process. New materials come out on a regular basis, but typically these are improvements replacing existing materials, not expanding choice. For SLA printing, the range of commercially available and custom-made materials are rapidly expanding, not only improving resolution[78] and chemical compatibility,[79] but also adding functionality including stretchability/gas permeability[80,81] and heat dissipation.[82] In this regard, the absence of biocompatible materials is a significant limitation, given the extensive and significant potential of microfluidics to study and replicate biological systems. Biocompatibility of photopolymers is another important issue, limiting the application of both inkjet and SLA-based methods in cell culture platforms.[83] Ong *et al.* presented microchannels yielding cell-spheroid viability over 72 h. This device, however, comprised multiple non-3D printed parts, including a glass slide to improve optical clarity, a PDMS layer for gas permeability, and screws to seal the glass slide to the 3D printed channels.[84] An extensive (multiple day) extraction method was demonstrated to be effective for the extraction of SLA-printed PDMS devices, with cell viability equivalent to cast PDMS after 72 h.[80]

In contrast, FDM printing has a good and growing selection of commercially available materials with different physical or mechanical properties, such as graphene contained conductive PLA for electronic printing,[85] iron contained magnetic PLA for magnets,[86] formulated flexible thermoplastic polyurethane (TPU) for gaskets and plugs,[87] most of which has been driven by the at-home and hobby market. Additionally, it is a relatively simple process to create your own custom filament through the use of a filament extruder to blend thermoplastics with other materials. Stability at extrusion temperatures (up to 240 °C) is required, but nanomaterials may be a thermostable alternative to enzymes, facilitating the integration of (bio)catalytic functionality. Research focusing on FDM printed formulations in the pharmaceutical industry is expected to enhance knowledge around the incorporation and controlled release of chemicals from FDM printed objects, and will accelerate the integration of reagent-releasing functionality in microchemical systems.[88]

No matter the printing approach, the adoption of novel, often research-grade materials in commercially viable 3D printed microchemical devices, however, is expected to be slow as the commercialization of the materials most likely will have to precede their use in commercial manufacture. The glass resin developed for SLA in 2017, however, is already commercially available now, and it will be interesting to see how this changes the field when used in a high resolution printer to create sub 20 μm channels in glass.[89]

To allow for 3D printing to grow from a rapid prototyping approach to a viable alternative for the fabrication of microchemical devices, the throughput needs to increase to meet the demands of industry for mass production. Current typical fabrication of a simple microfluidic device takes 4, 10 and 33 devices per hour for DLP–SLA, FDM and inkjet, respectively, which may limit the commercial viability of manufacturing devices.[24] For SLA, the continuous liquid interface production (CLIP) 3D printing technology by Tumbleston *et al.* facilitated the continuous generation of monolithic polymeric parts ten times quicker, with print speeds of hundreds of mm h^{-1}, demonstrating a technology solution that significantly increased the manufacturing potential of SLA printers.[90] While 30–40 devices an hour is much less than can be achieved using large volume manufacturing approaches, such as embossing and injection molding, it could facilitate the production of 2000 devices a week (100 000 per year). This production level is achieved using the same infrastructure basis for prototyping, without further investment, thus creating a potentially new approach for translation of devices into the market with reduce cost to build market, before moving to larger volume manufacturing.

The PPP approach provides an attractive hybrid solution combining 3D printed and other objects. SLA printing, while offering the highest resolution, requires embedded components to be compatible with the liquid-resin in which they will be submerged, limiting the selection of materials and components. The use of the support material in inkjet printing limits the PPP integration by inkjet printing to thin objects like membranes, as larger objects interfere with continuing the print process. FDM printing, in contrast, leaves voids making this printing technique the most attractive for PPP, and the only approach where embedding liquid/solids into microchannels created by the printer have been demonstrated.

The highest level of functional integration can be obtained by multimaterial 3D printing, but there are a number of challenges in addition to the those listed above. Having the highest resolution of the 3D printing methods, the easiest method for multimaterial SLA is using different resin vats. This approach was demonstrated Chio and co-workers with multimaterial stereolithography (MMSLA) machine containing 4 resins. While functional, the structure must be moved between each resin for printing each layer, thus the print time is at four times longer than a single material print and it is not compatible with the CLIP printing approach to improve speed.[91] Recent work from Hawker demonstrating optical-generation of different monomers in the SLA 3D print process could potentially change this, particularly if implemented in a CLIP-like system.[92] Multimaterial-inkjet based systems are much quicker, as the different materials can be printed in the same print pass for each layer.[93,94] For example, the Stratasys Objet Connex printers can print up to three different materials, and combinations of these, in a single run. However, there is a technical limitation in controlling the deposition process without blending of materials prior to curing, which resulted in the fine structures exploited by Macdonald *et al.* to create a porous chromatographic surface.[45] These issues will have to be overcome in order to use inkjet for the printing of electronics and sensors,

potentially even semiconductor devices, where purity of layers is critical. The work of Saleh *et al.* who demonstrated 3D printing of integrated electronic devices by combining UV sintering of a conductive ink based on silver nanoparticle (AgNP), with UV curing of an insulator to house the features is one potential solution to this problem.[95] Despite rapid development of materials in research organisations, warranty issues make it unattractive to print with custom materials due to the high cost of the printer and propriety nature of the hardware and print process. The availability of multi-head FDM printers as well as options in splicing filaments for multimaterial printing using a single nozzle printer make this technique currently best equipped for the fabrication of integrated chemical devices.[22] While technical limitations for multimaterial FDM printed are fewer, there are still issues with material compatibility, adhesion of one material to another and developing processes for the use of materials that extrude at significantly different temperatures. FDM printing however, is potentially the easiest to combine with bioprinting for the creation of devices that contain biological, chemical, electrical and mechanical functionality in a way that is currently not possible.

6. Conclusion

Limitations of traditional manufacturing methods for the fabrication of integrated microfluidic devices including expensive infrastructure, limited flexibility in design especially in the third dimension, limited choice of materials and time-intensive processing steps have raised interest in the use of advanced manufacturing methods. Functional integration in 3D printed microchemical systems can be grouped in three approaches: 1) functional integration by 3D spacing of material, 2) functional integration by incorporating external components (incl. liquid reagents) by print-pause-print (PPP) 3) functional integration by multimaterial 3D printing. The first approach relies on functionalities that scale with 3D geometry, and in addition to fluid dynamic functions, has led to the demonstration of fluidic functions (pumps, valves and mixers), porous, sorbent materials for chromatography and extraction, and the introduction of modular fluidic systems. The range of functionalities than can be realized through design using a single material, however, is limited. The second approach, based on in-print integration of 3D printed objects with external objects/functional elements using the PPP approach is popular because it allows for the integration of complex functionality without requiring significant changes to the 3D printing hardware. PPP has been used for the integration of electronics, chemical reagents and membranes. The third approach, multimaterial 3D printing allows for a high level of functional integration using a single, automated manufacturing step.

Multimaterial 3D printing is highly reliant on the availability of the appropriate technology and materials. Despite the superior resolution of SLA printers, its use for multimaterial printing is limited by material choice and lack of a suitable multimaterial printing approach. The propriety nature of inkjet 3D printers has limited the material choice, and restricted its use for multimaterial printing to combinations of flexible and rigid materials for fluidic control and sealing. FDM printing has a broad selection of materials as well as commercially available platforms for multimaterial printing, and exiting examples of integrating catalysts, electrodes and membranes have been presented.

For the deployment of Lab on a Chip systems, especially truly autonomous μTAS systems out of a laboratory setting, the reliance on external systems and components needs to be reduced/eliminated, increasing the demand for complex functional integration. Traditional manufacturing approaches struggle to meet the demand for the fabrication of complex, functionally integrated microchemical devices in a cost- and time effective manner. 3D printing may provide a cost-competitive alternative pathway, especially for rapid prototyping and low volume applications of highly integrated microchemical systems. Advances in 3D printing processes and materials are required and anticipated to accelerate the development of complex, integrated microchemical systems.

Conflicts of interest

There are no conflicts to declare.

Acknowledgements

F. L. acknowledges the University of Tasmania for the provision of a scholarship. M. C. B. acknowledges an Australian Research Council Future Fellowship award (FT130100101).

References

1 J. S. Kilby, *US Pat.*, 3138743A, 1964.
2 J. W. Judy, *Smart Mater. Struct.*, 2001, **10**, 1115.
3 A. R. Grayson, R. S. Shawgo, A. M. Johnson, N. T. Flynn, Y. Li, M. J. Cima and R. Langer, *Proc. IEEE*, 2004, **92**, 6–21.
4 A. Manz, N. Graber and H. Á. Widmer, *Sens. Actuators, B*, 1990, **1**, 244–248.
5 J.-W. Choi, K. W. Oh, J. H. Thomas, W. R. Heineman, H. B. Halsall, J. H. Nevin, A. J. Helmicki, H. T. Henderson and C. H. Ahn, *Lab Chip*, 2002, **2**, 27–30.
6 F. Li, R. M. Guijt and M. C. Breadmore, *Anal. Chem.*, 2016, **88**, 8257–8263.
7 A. I. Shallan, R. M. Guijt and M. C. Breadmore, *Angew. Chem.*, 2015, **127**, 7467–7470.
8 C. J. Easley, J. M. Karlinsey, J. M. Bienvenue, L. A. Legendre, M. G. Roper, S. H. Feldman, M. A. Hughes, E. L. Hewlett, T. J. Merkel and J. P. Ferrance, *Proc. Natl. Acad. Sci. U. S. A.*, 2006, **103**, 19272–19277.
9 E. Lagally, I. Medintz and R. Mathies, *Anal. Chem.*, 2001, **73**, 565–570.
10 E. T. Lagally, P. C. Simpson and R. A. Mathies, *Sens. Actuators, B*, 2000, **63**, 138–146.
11 H. Wei, H. Li and J.-M. Lin, *J. Chromatogr. A*, 2009, **1216**, 9134–9142.

12 B. Liu, Y. Zhang, D. Mayer, H. J. Krause, Q. Jin, J. Zhao and A. Offenhäusser, *Electrophoresis*, 2011, **32**, 699–704.
13 B. S. Broyles, S. C. Jacobson and J. M. Ramsey, *Anal. Chem.*, 2003, **75**, 2761–2767.
14 B. P. Mason, K. E. Price, J. L. Steinbacher, A. R. Bogdan and D. T. McQuade, *Chem. Rev.*, 2007, **107**, 2300–2318.
15 C. W. Shields IV, C. D. Reyes and G. P. López, *Lab Chip*, 2015, **15**, 1230–1249.
16 R. M. Guijt and A. Manz, *Sens. Actuators, B*, 2018, **273**, 1334–1345.
17 B. Gross, S. Y. Lockwood and D. M. Spence, *Anal. Chem.*, 2016, **89**, 57–70.
18 H. Becker, *Lab Chip*, 2009, **9**, 2759–2762.
19 I. Campbell, D. Bourell and I. Gibson, *Rapid Prototyp. J.*, 2012, **18**, 255–258.
20 I. Gibson, D. Rosen and B. Stucker, *Additive manufacturing technologies: 3D printing, rapid prototyping, and direct digital manufacturing*, Springer, 2014.
21 N. Bhattacharjee, A. Urrios, S. Kang and A. Folch, *Lab Chip*, 2016, **16**, 1720–1742.
22 S. Waheed, J.-M. Cabot Canyelles, N. Macdonald, R. M. Guijt, T. Lewis, B. Paull and M. C. Breadmore, *Lab Chip*, 2016, **16**, 1993–2013.
23 M. Vaezi, S. Chianrabutra, B. Mellor and S. Yang, *Virtual Phys. Prototyp.*, 2013, **8**, 19–50.
24 N. P. Macdonald, J. M. Cabot, P. Smejkal, R. M. Guijt, B. Paull and M. C. Breadmore, *Anal. Chem.*, 2017, **89**, 3858–3866.
25 C. Pinger, A. Heller and D. M. Spence, *Anal. Chem.*, 2017, **89**, 7302–7306.
26 C. I. Rogers, K. Qaderi, A. T. Woolley and G. P. Nordin, *Biomicrofluidics*, 2015, **9**, 016501.
27 H. Gong, A. T. Woolley and G. P. Nordin, *Lab Chip*, 2016, **16**, 2450–2458.
28 A. K. Au, N. Bhattacharjee, L. F. Horowitz, T. C. Chang and A. Folch, *Lab Chip*, 2015, **15**, 1934–1941.
29 R. Sochol, E. Sweet, C. Glick, S. Venkatesh, A. Avetisyan, K. Ekman, A. Raulinaitis, A. Tsai, A. Wienkers and K. Korner, *Lab Chip*, 2016, **16**, 668–678.
30 J. Wang, C. McMullen, P. Yao, N. Jiao, M. Kim, J.-W. Kim, L. Liu and S. Tung, *Microfluid. Nanofluid.*, 2017, **21**, 105.
31 H. N. Chan, Y. Shu, B. Xiong, Y. Chen, Y. Chen, Q. Tian, S. A. Michael, B. Shen and H. Wu, *ACS Sens.*, 2015, **1**, 227–234.
32 P. Hinsmann, J. Frank, P. Svasek, M. Harasek and B. Lendl, *Lab Chip*, 2001, **1**, 16–21.
33 Y. Song, J. Hormes and C. S. Kumar, *Small*, 2008, **4**, 698–711.
34 J. Pihl, J. Sinclair, E. Sahlin, M. Karlsson, F. Petterson, J. Olofsson and O. Orwar, *Anal. Chem.*, 2005, 77, 3897–3903.
35 G. H. Seong and R. M. Crooks, *J. Am. Chem. Soc.*, 2002, **124**, 13360–13361.
36 A. D. Stroock, S. K. Dertinger, A. Ajdari, I. Mezić, H. A. Stone and G. M. Whitesides, *Science*, 2002, **295**, 647–651.
37 K. Plevniak, M. Campbell, T. Myers, A. Hodges and M. He, *Biomicrofluidics*, 2016, **10**, 054113.
38 A. I. Shallan, P. Smejkal, M. Corban, R. M. Guijt and M. C. Breadmore, *Anal. Chem.*, 2014, **86**, 3124–3130.
39 P. Carrière, *Phys. Fluids*, 2007, **19**, 118110.
40 J. M. Cabot, E. Fuguet, M. Roses, P. Smejkal and M. C. Breadmore, *Anal. Chem.*, 2015, **87**, 6165–6172.
41 F. Li, N. P. Macdonald, R. M. Guijt and M. C. Breadmore, *Anal. Chem.*, 2017, **89**, 12805–12811.
42 C.-K. Su, P.-J. Peng and Y.-C. Sun, *Anal. Chem.*, 2015, **87**, 6945–6950.
43 D. Fichou and G. E. Morlock, *Anal. Chem.*, 2017, **89**, 2116–2122.
44 M. Belka, S. Ulenberg and T. Bączek, *Anal. Chem.*, 2017, **89**, 4373–4376.
45 N. P. Macdonald, S. A. Currivan, L. Tedone and B. Paull, *Anal. Chem.*, 2017, **89**, 2457–2463.
46 K. G. Lee, K. J. Park, S. Seok, S. Shin, J. Y. Park, Y. S. Heo, S. J. Lee and T. J. Lee, *RSC Adv.*, 2014, **4**, 32876–32880.
47 K. C. Bhargava, B. Thompson and N. Malmstadt, *Proc. Natl. Acad. Sci. U. S. A.*, 2014, **111**, 15013–15018.
48 P. K. Yuen, *Lab Chip*, 2008, **8**, 1374–1378.
49 P. K. Yuen, *Lab Chip*, 2016, **16**, 3700–3707.
50 E. MacDonald and R. Wicker, *Science*, 2016, **353**, aaf2093.
51 G. Scotti, S. M. E. Nilsson, M. Haapala, P. Poho, G. Boije af Gennas, J. Yli-Kauhaluoma and T. Kotiaho, *React. Chem. Eng.*, 2017, **2**, 299–303.
52 G. Gaal, M. Mendes, T. P. de Almeida, M. H. O. Piazzetta, Â. L. Gobbi, A. Riul Jr and V. Rodrigues, *Sens. Actuators, B*, 2017, **242**, 35–40.
53 M. Banna, K. Bera, R. Sochol, L. Lin, H. Najjaran, R. Sadiq and M. Hoorfar, *Sensors*, 2017, **17**, 1336.
54 P. J. Kitson, M. H. Rosnes, V. Sans, V. Dragone and L. Cronin, *Lab Chip*, 2012, **12**, 3267–3271.
55 P. J. Kitson, R. J. Marshall, D. Long, R. S. Forgan and L. Cronin, *Angew. Chem., Int. Ed.*, 2014, **53**, 12723–12728.
56 P. J. Kitson, M. D. Symes, V. Dragone and L. Cronin, *Chem. Sci.*, 2013, **4**, 3099–3103.
57 F. Lederle, F. Meyer, C. Kaldun, J. C. Namyslo and E. G. Hübner, *New J. Chem.*, 2017, **41**, 1925–1932.
58 P. K. Yuen, *Biomicrofluidics*, 2016, **10**, 044104.
59 S. Begolo, D. V. Zhukov, D. A. Selck, L. Li and R. F. Ismagilov, *Lab Chip*, 2014, **14**, 4616–4628.
60 E. Jue, N. G. Schoepp, D. Witters and R. F. Ismagilov, *Lab Chip*, 2016, **16**, 1852–1860.
61 S. J. Keating, M. I. Gariboldi, W. G. Patrick, S. Sharma, D. S. Kong and N. Oxman, *PLoS One*, 2016, **11**, e0160624.
62 L. C. Duarte, C. L. S. Chagas, L. E. B. Ribeiro and W. K. T. Coltro, *Sens. Actuators, B*, 2017, **251**, 427–432.
63 Z. Rymansaib, P. Iravani, E. Emslie, M. Medvidović-Kosanović, M. Sak-Bosnar, R. Verdejo and F. Marken, *Electroanalysis*, 2016, **28**, 1517–1523.
64 S. J. Leigh, R. J. Bradley, C. P. Purssell, D. R. Billson and D. A. Hutchins, *PLoS One*, 2012, **7**, e49365.
65 S. J. Leigh, C. P. Purssell, D. R. Billson and D. A. Hutchins, *Smart Mater. Struct.*, 2014, **23**, 095039.
66 S. Phung, presented in part at *MicroTAS 2016*, Dublin, October 2016.
67 J. S. Park, T. Kim and W. S. Kim, *Sci. Rep.*, 2017, **7**, 3246.

68 V. G. Rocha, E. García-Tuñón, C. Botas, F. Markoulidis, E. Feilden, E. D'Elia, N. Ni, M. Shaffer and E. Saiz, *ACS Appl. Mater. Interfaces*, 2017, **9**, 37136–37145.
69 M. D. Symes, P. J. Kitson, J. Yan, C. J. Richmond, G. J. Cooper, R. W. Bowman, T. Vilbrandt and L. Cronin, *Nat. Chem.*, 2012, **4**, 349.
70 F. Li, P. Smejkal, N. P. Macdonald, R. M. Guijt and M. C. Breadmore, *Anal. Chem.*, 2017, **89**, 4701–4707.
71 C.-K. Su and J.-C. Chen, *Anal. Chim. Acta*, 2018, **1036**, 133–140.
72 S. Y. Lockwood, J. E. Meisel, F. J. Monsma and D. M. Spence, *Anal. Chem.*, 2016, **88**, 1864–1870.
73 O. Paydar, C. Paredes, Y. Hwang, J. Paz, N. Shah and R. Candler, *Sens. Actuators, A*, 2014, **205**, 199–203.
74 S. A. Gowers, V. F. Curto, C. A. Seneci, C. Wang, S. Anastasova, P. Vadgama, G.-Z. Yang and M. G. Boutelle, *Anal. Chem.*, 2015, **87**, 7763–7770.
75 G. W. Bishop, J. Satterwhite, S. Bhakta, K. Kadimisetty, K. M. Gillette, E. Chen and J. F. Rusling, *Anal. Chem.*, 2015, **87**, 5437–5443.
76 Q. Ji, J. M. Zhang, Y. Liu, X. Li, P. Lv, D. Jin and H. Duan, *Sci. Rep.*, 2018, **8**, 4791.
77 S. Maruo, O. Nakamura and S. Kawata, *Opt. Lett.*, 1997, **22**, 132–134.
78 H. Gong, B. P. Bickham, A. T. Woolley and G. P. Nordin, *Lab Chip*, 2017, **17**, 2899–2909.
79 F. Kotz, K. Arnold, W. Bauer, D. Schild, N. Keller, K. Sachsenheimer, T. M. Nargang, C. Richter, D. Helmer and B. E. Rapp, *Nature*, 2017, **544**, 337.
80 N. Bhattacharjee, C. Parra-Cabrera, Y. T. Kim, A. P. Kuo and A. Folch, *Adv. Mater.*, 2018, **30**, 1800001.
81 T. Femmer, A. J. Kuehne and M. Wessling, *Lab Chip*, 2014, **14**, 2610–2613.
82 S. Waheed, J. M. Cabot, N. P. Macdonald, U. Kalsoom, S. Farajikhah, P. C. Innis, P. N. Nesterenko, T. W. Lewis, M. C. Breadmore and B. Paull, *Sci. Rep.*, 2017, **7**, 15109.
83 N. P. Macdonald, F. Zhu, C. Hall, J. Reboud, P. Crosier, E. Patton, D. Wlodkowic and J. Cooper, *Lab Chip*, 2016, **16**, 291–297.
84 L. J. Y. Ong, A. B. Islam, R. DasGupta, N. G. Iyer, H. L. Leo and Y.-C. Toh, *Biofabrication*, 2017, **9**, 045005.
85 http://www.blackmagic3d.com/Conductive-p/grphn-pla.htm.
86 https://www.proto-pasta.com/products/magnetic-iron-pla.
87 https://ninjatek.com/products/filaments/ninjaflex/.
88 A. Awad, S. J. Trenfield, S. Gaisford and A. W. Basit, *Int. J. Pharm.*, 2018, **548**, 586–596.
89 http://glassomer.com/.
90 J. R. Tumbleston, D. Shirvanyants, N. Ermoshkin, R. Janusziewicz, A. R. Johnson, D. Kelly, K. Chen, R. Pinschmidt, J. P. Rolland, A. Ermoshkin, E. T. Samulski and J. M. DeSimone, *Science*, 2015, **347**, 1349–1352.
91 J.-W. Choi, H.-C. Kim and R. Wicker, *J. Mater. Process. Technol.*, 2011, **211**, 318–328.
92 N. D. Dolinski, Z. A. Page, E. B. Callaway, F. Eisenreich, R. V. Garcia, R. Chavez, D. P. Bothman, S. Hecht, F. W. Zok and C. J. Hawker, *Adv. Mater.*, 2018, 1800364.
93 J. Visser, B. Peters, T. J. Burger, J. Boomstra, W. J. Dhert, F. P. Melchels and J. Malda, *Biofabrication*, 2013, **5**, 035007.
94 S. V. Murphy and A. Atala, *Nat. Biotechnol.*, 2014, **32**, 773.
95 E. Saleh, F. Zhang, Y. He, J. Vaithilingam, J. L. Fernandez, R. Wildman, I. Ashcroft, R. Hague, P. Dickens and C. Tuck, *Adv. Mater. Technol.*, 2017, **2**, 1700134.